

High-Performance Organic Thermoelectric Materials: Theoretical Insights and Computational Design

Wen Shi, Dong Wang,* and Zhigang Shuai*

Eco-friendly and high-performance thermoelectric materials that interconvert heat and electricity based on the Seebeck effect and Peltier effect are urgently needed due to their enormous potential in solid-state power generation and refrigeration. Recently, revolutionary advances driven by experiments are made in developing innovative organic thermoelectric materials. Meantime, with the help of state-of-the-art first-principles calculations, theoretical understanding and rational design of organic thermoelectric materials are emerging. This review presents the authors' current progress achieved in design strategies for high-performance organic thermoelectric materials at the level of atomistic simulation. The in-depth understanding gained in these explorations will help to build the fundamental structure–property relationship, and in turn promote the development of next-generation high-performance organic thermoelectric materials.

possess decent Seebeck coefficient, high conductivity, and poor thermal conductivity, which is known as the “phonon-glass, electron-crystal” criterion.^[4] This far-reaching concept has thoroughly changed our thinking in the design of TE materials but unfortunately the development of high-performance TE materials has been a tremendous challenge mainly because TE transport coefficients are inter-related and often contradicted with each other. For instance, with the conductivity increasing the Seebeck coefficient decreases dramatically, and the electronic thermal conductivity also increases.^[5] So far, two successful strategies, which include the lattice thermal conductivity suppression and the electronic band structure engineering, have been proposed

1. Introduction

Thermoelectric (TE) materials—one of the solid-state energy solutions enabling direct heat–electricity conversion are believed to be promising in the field of power generation and refrigeration.^[1] To compete with other types of clean energy solutions, the energy conversion efficiency of TE generators and refrigerators needs to be substantially improved.^[2] The dimensionless TE figure of merit of a material is defined as $zT = S^2\sigma T/\kappa$, where S is the Seebeck coefficient (i.e., the thermopower); σ is the electrical conductivity; $S^2\sigma$ is called the power factor; T is the absolute temperature; κ is the total thermal conductivity. In solid-state materials, both electrons (κ_e) and lattice vibrations (κ_l) carry heat, so both of them contribute to the total thermal conductivity, namely, $\kappa = \kappa_e + \kappa_l$.^[3] A TE material with high figure of merit must simultaneously


to enhance the figure of merit of TE materials.^[6] Up to now, quite few TE materials with decent figure of merit (close to unity) near ambient temperature have been reported, except for Bi_2Te_3 and alloys^[7] which however contain tellurium—one of the rarest elements on earth, and their fabrication requires extremely demanding vacuum processing technology.

Meanwhile, the 20th century has witnessed a great revolution in organic electronics, starting with the discovery of conducting polymers.^[8] Organic electronic materials are flexible, inexpensive, printable, easy to manufacture, and importantly have relatively low lattice thermal conductivity, which positions them in an advantageous place over conventional inorganic electronic materials for near-ambient TE applications.^[9] With the benefit of advanced synthesis and characterization techniques, tremendous breakthrough has been made in the development of high-performance organic TE materials since 2010,^[10] especially polymeric TE materials.^[11] Among them, poly(3,4-ethylenedioxythiophene) (PEDOT) is known to be one of the best p-type organic TE materials.^[12] The PEDOT thin films with *p*-toluenesulfonate (Tos) as counter anions showed a decent room-temperature p-type figure of merit of 0.25,^[13] and those with poly(styrenesulphonate) (PSS) as counter anions exhibited a high figure of merit of 0.42.^[14] Additionally, transition-metal coordination polymers show fascinating n-type TE performance.^[15] For instance, the n-type figure of merit of poly(nickel-ethylenetetra-thiolate) [poly(Ni-ett)] thin films with potassium counter cations reached 0.32 at 400 K,^[16] and its powder exhibited a high figure of merit of 0.2 at 440 K.^[17]

Despite these progress, there is a long way to go for the development of organic TE materials with even higher figure of merit. For a long time, tuning TE properties has been an endeavor driven by experiments, and to achieve decent

Dr. W. Shi, Prof. D. Wang, Prof. Z. G. Shuai
MOE Key Laboratory of Organic OptoElectronics
and Molecular Engineering
Department of Chemistry
Tsinghua University
Beijing 100084, P. R. China
E-mail: dong913@tsinghua.edu.cn; zgshuai@tsinghua.edu.cn

Prof. Z. G. Shuai
Key Laboratory of Organic Solids
Beijing National Laboratory for Molecular Science (BNLMS)
Institute of Chemistry
Chinese Academy of Sciences
Beijing 100190, P. R. China

 The ORCID identification number(s) for the author(s) of this article can be found under <https://doi.org/10.1002/aelm.201800882>.

DOI: 10.1002/aelm.201800882

performance in organic TE materials, efforts have been devoted to regulating the carrier concentration via chemical doping^[18] or field-effect modulation,^[19] controlling the microscopic morphology,^[20] engineering the chemical structure,^[21] changing the size of the counterion,^[22] etc. To help with the rational design of high-performance organic TE materials, theoretical understandings of TE conversion are indispensable since they can shed light on the fundamental charge and heat transport processes, and bridge the gap between microscopic chemical structures and macroscopic TE transport properties. With the advancement of electronic structure methods and large-scale molecular dynamics simulations, a new era of designing organic TE materials aided by theoretical computations is emerging. Over the last decade, we have developed a parameter-free computational scheme to predict TE properties of organic materials,^[23] which combines density functional theory (DFT) calculations for band structures, Boltzmann transport theory for electrical transport coefficients,^[24] deformation potential (DP) theory^[25] for electron–phonon scatterings, and nonequilibrium molecular dynamics (NEMD) simulations for phonon transport properties. The related methodologies and computational scheme have been summarized in a recent review^[26] and an earlier one.^[27] This scheme is now widely exploited and has been proven to be robust in predicting the mobility of 1D^[28] or 2D carbon-based materials^[29] and organic single crystals,^[30] TE properties of organic molecular crystals,^[31] crystalline conjugated polymers,^[32] organic–inorganic hybrid perovskites,^[33] transition-metal coordination polymers,^[34] and thermal conductivity of organic molecular crystals.^[35] In this review, we will not focus on the methodology development, but rather provide new understandings and design strategies for high-performance organic TE materials gained from these state-of-the-art theoretical calculations. In Section 2, we will take 2,7-dialkyl[1]benzothieno[3,2-b][1]benzothiophene derivatives (C_n -BTBTs) as an example to explore the TE conversion in small-molecule organic semiconductors. In Section 3, we will discuss the TE conversion in conducting polymers, PEDOT:Tos. Main conclusions and outlooks will be provided in the last section.

2. TE Conversion in Small-Molecule Organic Semiconductors: C_n -BTBTs

The Seebeck coefficients of small-molecule organic semiconductors, including both crystalline rubrene and pentacene films, were measured with field-effect transistors by Batlogg and co-workers, and decent values in the range of 0.3–1 mV K⁻¹ were obtained between 200 and 295 K.^[19] Besides, the thermal conductivities of both pentacene thin films^[36] and crystalline rubrene^[37] were reported to be about 0.5 W m⁻¹ K⁻¹ at room temperature. The high Seebeck coefficient and low thermal conductivity indicate that these small-molecule organic semiconductors might be promising TE materials. Meanwhile, our computational investigations also demonstrated that some prototypical molecular crystals, including pentacene, rubrene,^[38] and phthalocyanine,^[23] indeed exhibited decent TE performance. For organic small-molecule semiconductors, the precise control of carrier concentration via intentional doping is inevitable in order to increase their conductivity, however



Wen Shi received his Ph.D. in physical chemistry supervised by Prof. Zhigang Shuai and Prof. Dong Wang in the Department of Chemistry, Tsinghua University, Beijing, China in 2017. He graduated with a B.S. degree majoring in chemistry from Department of Chemistry, China Agricultural University, Beijing, China in 2012. His current research interests are theoretical investigations on organic and organic–inorganic hybrid thermoelectric materials and understanding the charge and heat transport in organic and organic–inorganic hybrid electronic materials from first principles.



Dong Wang received her Ph.D. in physical chemistry from the University of Science and Technology of China in 2000. Thereafter, she worked as a postdoctoral research associate with Prof. Eitan Geva at the University of Michigan and with Prof. Greg Voth at the University of Utah. In 2010, she joined the faculty of Department of Chemistry, Tsinghua University as an associate professor. Her current research interests include theoretical understanding of the thermoelectric process in novel organic and hybrid materials, and computer simulation of self-assembly in solution and on surface.



Zhigang Shuai got his Ph.D. degree from Fudan University with Prof. Xin Sun in 1989. Then he did postdoc with Prof. Jean-Luc Brédas in the University of Mons, Belgium. He is now Changjiang Scholar Professor in the Department of Chemistry, Tsinghua University. His research interests focus on the development of computational methodologies for describing the excited state electronic structures and dynamics applied to molecular/polymeric materials.

efficient doping is quite difficult because effective molecular dopants are lacking. More seriously, the dopants might alter the well-ordered molecular packings and thereby destroy the conduction pathways of charge carriers. To avoid this, a bilayer structure consisting of a pentacene layer and a dopant

layer of 2,3,5,6-tetrafluoro-7,7,8,8-tetracyanoquinodimethane (F₄-TCNQ) was developed, which showed the room-temperature conductivity of 0.43 S cm⁻¹, Seebeck coefficient of 0.2 mV K⁻¹, and power factor of 2.0 μW m⁻¹ K⁻².^[39] Yet, such level of doping and conductivity are too low for TE applications. Therefore, we propose to search for organic TE materials with high intrinsic mobility, and to verify our idea, we investigate from first principles the TE properties of a class of excellent hole transport organic semiconductors, C_n-BTBTs (*n* = 8, 10, 12).

2.1. Searching for Organic TE Materials with High Intrinsic Mobility

To illustrate the importance of searching for organic semiconductors with high intrinsic mobility as potential TE materials, we first derive a simple analytic equation based on the assumption of low carrier concentration and one conduction band,^[40] which gives the relationship between the maximum figure of merit, zT_{\max} and the intrinsic mobility, μ , as well as the lattice thermal conductivity, κ_L

$$zT_{\max} = \frac{4k_B^2 T \mu}{e} \frac{\left[L_0 e T \left(\frac{\mu}{\kappa_L} \right) N_{\text{opt}} + 1 \right]^2 N_{\text{opt}}}{L_0 e T \mu N_{\text{opt}} + \kappa_L} \quad (1)$$

where the optimal carrier concentration, N_{opt} satisfies $\ln N_{\text{opt}} = -2L_0 e T \left(\frac{\mu}{\kappa_L} \right) N_{\text{opt}} + \ln N_{\text{eff}} - 2$. Here, L_0 is the Sommerfeld value of Lorentz number, $(\pi^2/3)(k_B/e)^2 \approx 2.44 \times 10^{-8} \text{ W } \Omega^{-1} \text{ K}^{-2}$, and N_{eff} is the effective density of states. Obviously, a high intrinsic mobility combined with a low lattice thermal conductivity results in a low optimal carrier concentration (Figure 1a), which implies that less dopants are needed, and in such case the negative influence of dopants on charge transport can be minimized. More importantly, a high intrinsic mobility and a low lattice thermal conductivity also give rise to a high maximum figure of merit (Figure 1b). To be specific, the maximum figure of merit can easily reach 0.5, if the mobility is 10 cm² V⁻¹ s⁻¹ and the lattice thermal conductivity is

0.2 W m⁻¹ K⁻¹. Very recently, based on the same assumption, a formula has been derived to show the relationship between the maximum power factor, $(S^2\sigma)_{\max}$ and the intrinsic mobility, μ , which is $(S^2\sigma)_{\max} = (4k_B^2/e) \mu \exp(\ln N_{\text{eff}} - 2)$. This equation also emphasizes that it is crucial to search for high-mobility semiconductors for TE applications, since the maximum power factor is directly proportional to the intrinsic mobility.^[41]

Newly discovered small-molecule semiconductors, C_n-BTBTs (Figure 2a) possess excellent hole transport properties at room temperature.^[42] For example, the crystalline C₈-BTBT exhibited a high field-effect mobility of 31.3 cm² V⁻¹ s⁻¹.^[43] A blended thin film of C₈-BTBT and polystyrene showed an ultrahigh field-effect mobility of 43 cm² V⁻¹ s⁻¹.^[44] Also, band transport behavior was found in crystalline C_n-BTBTs. For instance, the mobility of crystalline C₈-BTBT decreased as the temperature increased from 160 to 300 K.^[45] Taking an ultimate monolayer of C₈-BTBT molecules as the thin-film transistor channel material, remarkable intrinsic mobility over 30 cm² V⁻¹ s⁻¹ and band transport behavior in the temperature range from 150 to 300 K were demonstrated.^[46] Terahertz electromodulation spectroscopic study also indicates that the crystalline C₁₂-BTBT showed band-like transport properties at room temperature.^[47]

The conjugated cores of crystalline C_n-BTBTs exhibited a herringbone packing motif in the *ab*-plane (Figure 2b). The alkyl side chain layers and the conjugated backbone layers align alternately along the *c*-axis, forming a typical lamella-like structure (Figure 2c). It is interesting to find that both lattice parameters *a* and *b* get smaller as the alkyl side chains become longer (Table 1) because hydrophobic interactions between longer alkyl side chains are stronger.^[50] As an example, the band structure of crystalline C₈-BTBT is shown in Figure 2d.

Based on Boltzmann transport theory^[24] and DP approximation,^[25] we calculated the electrical transport properties for crystalline C_n-BTBTs. The hole mobilities apparently show isotropic character in the *ab*-plane (Table 2), which is consistent with the field-effect results by Bao and co-workers.^[44] Interestingly, the hole mobilities increase as the alkyl side chains are elongated, which agrees with the experimental trend.^[50] The predicted hole mobility of C₈-BTBT (180 and 165 cm² V⁻¹ s⁻¹ along *a*- and *b*-axes, respectively) is about 5–6 times larger than the available

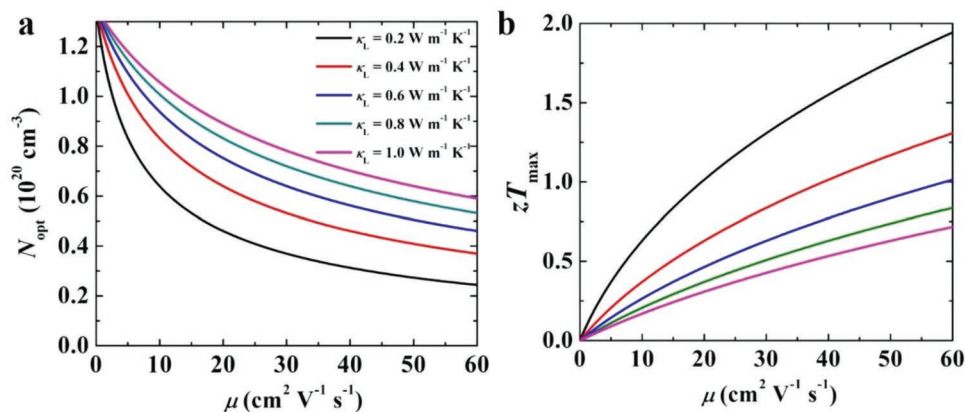


Figure 1. Dependence of a) the optimal carrier concentration, N_{opt} , and b) the maximum value of figure of merit, zT_{\max} on the charge carrier mobility, μ , as well as the lattice thermal conductivity, κ_L at room temperature. All panels reproduced with permission.^[31] Copyright 2014, American Chemical Society.

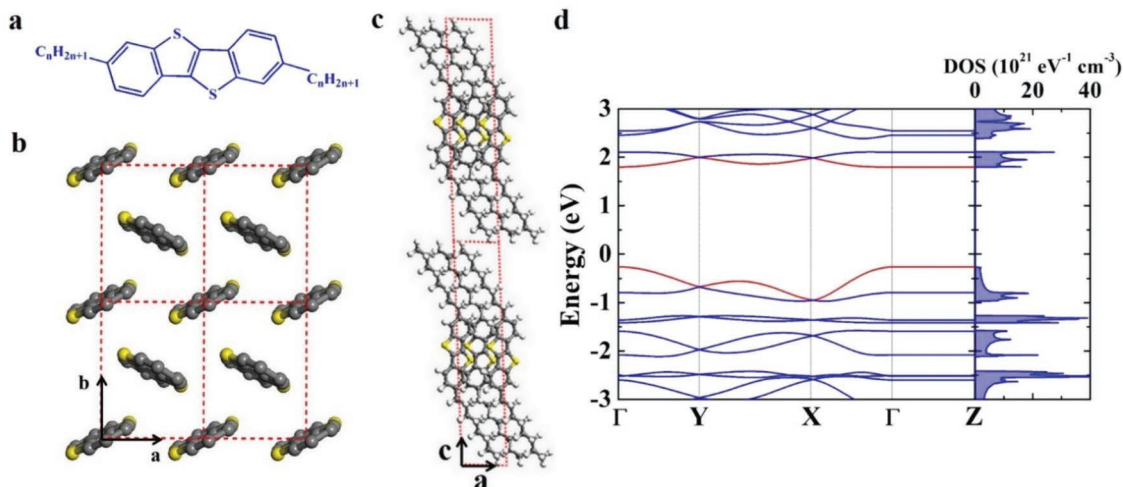


Figure 2. a) Chemical structure of C_n-BTBTs. b) Herringbone arrangement of crystalline C₈-BTBT in the *ab*-plane. The alkyl side chains and hydrogen atoms are not displayed. c) Lamella-like alternating structure of crystalline C₈-BTBT in the *ac*-plane. The red dashed lines represent the crystal lattices. d) Band structure and density of states (DOS) of C₈-BTBT. The reciprocal coordinates of high-symmetry points are $\Gamma = (0, 0, 0)$, $Y = (0, 0.5, 0)$, $X = (0.5, 0, 0)$, and $Z = (0, 0, 0.5)$, respectively. All panels reproduced with permission.^[31] Copyright 2014, American Chemical Society.

experimental data ($31.3 \text{ cm}^2 \text{ V}^{-1} \text{ s}^{-1}$).^[43] However, very recently an unprecedentedly high mobility of $170 \text{ cm}^2 \text{ V}^{-1} \text{ s}^{-1}$ was reported for C₁₂-BTBT measured with the field-induced time-resolved microwave conductivity technique,^[51] which is nearly the same with our prediction (211 and $199 \text{ cm}^2 \text{ V}^{-1} \text{ s}^{-1}$ along *a*- and *b*-axes, respectively) (Table 2). Also notably, our prediction of Seebeck coefficients at hole concentrations of 3×10^{18} to $1 \times 10^{19} \text{ cm}^{-3}$ has been verified by the subsequent experimental measurement by Sirringhaus and co-workers (Figure 3a), with deviations at lower hole concentrations attributed to the charge trapping.^[52] The hole conductivities, power factors, and electronic thermal conductivities of crystalline C₈-BTBT are almost isotropic in the *ab*-plane (Figure 3b–d).

In addition to introducing long alkyl side chains, novel approaches exploiting the inherent softness of organic small-molecule semiconductors, which include solution shearing method,^[53] application of uniaxial strain,^[54] and hydrostatic pressure,^[55] can subtly regulate the microscopic molecular packing structure, and then improve the charge carrier mobility. With the mobility enhanced, not only the optimal doping level is reduced, but also the power factor and figure of merit are improved.

Table 1. Lattice parameters for C_n-BTBTs optimized by the Perdew-Burke-Ernzerhof (PBE) exchange correlation functional^[48] with dispersion correction^[49] and those from experimental crystal structures. $\alpha = \gamma = 90^\circ$. Adapted with permission.^[31] Copyright 2014, American Chemical Society.

		<i>a</i> [Å]	<i>b</i> [Å]	<i>c</i> [Å]	β [°]
C ₈ -BTBT	Cal.	5.734	7.362	28.60	93.71
	Exp. ^[50]	5.927	7.880	29.18	92.44
C ₁₀ -BTBT	Cal.	5.725	7.262	32.88	85.53
	Exp. ^[50]	5.923	7.838	33.78	93.73
C ₁₂ -BTBT	Cal.	5.717	7.241	37.26	95.97
	Exp. ^[50]	5.864	7.740	37.91	90.59

2.2. Side Chain Engineering toward Reduced Lattice Thermal Conductivity

The long alkyl side chains of C_n-BTBTs not only make the conjugated cores pack more closely leading to the enhanced mobility, but also regulate the lattice thermal conductivity. We applied the classical NEMD approach with the general AMBER force field (GAFF)^[56] to derive the lattice thermal conductivity of crystalline C_n-BTBTs.^[57] The lattice thermal conductivities of C_n-BTBTs fall into the range of $0.18\text{--}0.25 \text{ W m}^{-1} \text{ K}^{-1}$ (Figure 4), demonstrating a typical glass-like thermal transport. Such poor thermal transport behavior originates from the weak intermolecular van der Waals interactions in these organic solids, and accordingly, crystalline molecular materials are also called “phonon-glass crystals.”^[58] The lattice thermal conductivity of crystalline C_n-BTBTs is even smaller than most advanced inorganic TE materials. For example, the room-temperature lattice thermal conductivity of PbTe was suppressed to about $0.6 \text{ W m}^{-1} \text{ K}^{-1}$ based on the all-scale hierarchical architecture approach.^[59] Recently, it was reported that layered SnSe crystals possessed poor out-of-plane lattice thermal conductivity of $0.9 \text{ W m}^{-1} \text{ K}^{-1}$ at room temperature.^[60]

As yet, no experimental thermal conductivity of C_n-BTBTs has been reported, but thermal conductivities of several other organic small-molecule thin films have been

Table 2. Hole relaxation time, τ and mobility, μ for C_n-BTBTs along the *a*- and *b*-axes at room temperature. The experimental mobility for C₁₂-BTBT is shown for comparison. Adapted with permission.^[31] Copyright 2014, American Chemical Society.

	C ₈ -BTBT	C ₁₀ -BTBT	C ₁₂ -BTBT
τ [fs]	117	127	136
μ_a [$\text{cm}^2 \text{ V}^{-1} \text{ s}^{-1}$]	180.3	194.1	211.0
μ_b [$\text{cm}^2 \text{ V}^{-1} \text{ s}^{-1}$]	165.1	174.3	199.2
μ [$\text{cm}^2 \text{ V}^{-1} \text{ s}^{-1}$] (Exp.) ^[51]			170

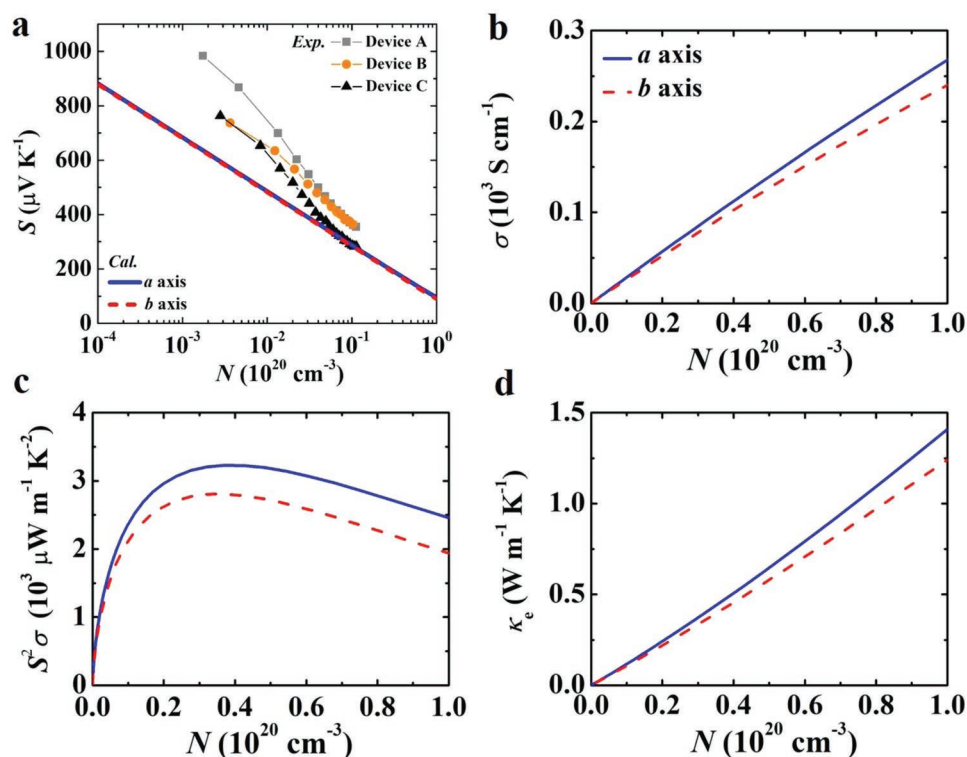


Figure 3. a) Seebeck coefficient, S , b) conductivity, σ , c) power factor, $S^2\sigma$, and d) electronic thermal conductivity, κ_e along the a - and b -axes of C_8 -BTBT varying with the hole concentration, N at room temperature. The experimental Seebeck coefficients taken from ref. [52] are shown for comparison. All panels reproduced with permission.^[31] Copyright 2014, American Chemical Society.

measured, including pentacene ($0.51 \text{ W m}^{-1} \text{ K}^{-1}$), N,N' -diphenyl- N,N' -di(3-methylphenyl)-(1,1'-biphenyl)-4,4'-diamine ($0.24 \text{ W m}^{-1} \text{ K}^{-1}$), and tris(8-hydroquinolinato)aluminum ($0.48 \text{ W m}^{-1} \text{ K}^{-1}$) (Figure 4).^[36] The predicted thermal conductivities of crystalline C_n -BTBTs are the smallest among these molecular materials, reaching a lower limit. The suppression of lattice thermal conductivity in C_n -BTBTs can be attributed to the long alkyl side chains, which have introduced many low-frequency vibrational modes and increased the probability of low-frequency phonon scattering. Previously, we predicted the lattice thermal conductivity for pentacene single crystals to be 0.72, 1.1, and $0.61 \text{ W m}^{-1} \text{ K}^{-1}$ in the three reciprocal lattice directions, respectively,^[35] and the value for metal-free phthalocyanine single crystals to be $2.1 \text{ W m}^{-1} \text{ K}^{-1}$ in the closest stacking direction.^[23] We find that by introducing long alkyl side chains into C_n -BTBTs, 4–10 times reduction of lattice thermal conductivity is achieved, which in turn will enhance the TE figure of merit. Similar to the electrical transport, the lattice thermal transport in crystalline C_n -BTBTs exhibits little anisotropy (Figure 4).

As provided in Table 3, the peak values of figure of merit for C_8 -, C_{10} -, and C_{12} -BTBTs are 2.4, 2.4, and 2.6 along the a -axis at the optimal hole concentration of 9.8×10^{18} , 9.3×10^{18} , and $11 \times 10^{18} \text{ cm}^{-3}$, respectively, and those along the b -axis are 2.2, 2.1, and 1.8 at the optimal hole concentration of 9.8×10^{18} , 9.3×10^{18} , and $9.3 \times 10^{18} \text{ cm}^{-3}$, respectively. Here, we did not consider the influence of dopants on the TE transport coefficients, so the figure of merit reported is undoubtedly overestimated. Our point is that introduction of long alkyl side chains is indeed an effective strategy to improve the TE performance,

because on one hand the mobility increases due to more closely packed conjugated backbones, and on the other hand by introducing plenty of low-frequency phonon modes, the lattice thermal conductivity is suppressed to an extremely low level (0.18 – $0.25 \text{ W m}^{-1} \text{ K}^{-1}$). In a word, we expect high-mobility small-molecule organic semiconductors such as C_n -BTBTs to showcase outstanding TE properties as long as efficient doping of these semiconductors can be realized.

3. TE Conversion in Conducting Polymers: PEDOT:Tos

3.1. Chemical Doping Effect on TE Conversion in PEDOT:Tos

Usually, chemical doping of TE polymers has the so-called “double-edged sword” effect, and hereafter we call it “doping dilemma.” On one hand, the figure of merit can be optimized with the help of subtly tuning carrier concentration through chemical doping. One representative experimental example is that through step-by-step chemical reduction of PEDOT:Tos with tetrakis(dimethylamino)ethylene vapor, a high zT of 0.25 was achieved at room temperature.^[13] On the other hand, the presence of dopants or counterions can destroy the well-ordered stacking structures of host polymers, reduce the mobility of charge carriers, and eventually deteriorate the TE performance. As an example, by removing the nonionized doping species from PEDOT:PSS using hydrophilic solvents, such as ethylene glycol and dimethylsulfoxide, an originally low power factor of about

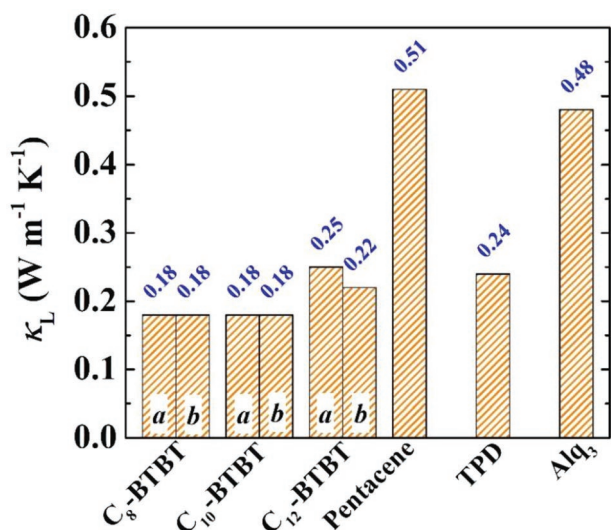


Figure 4. Lattice thermal conductivity, κ_L of C_n -BTBTs along the a - and b -axes at room temperature. Experimental results for small-molecule organic materials, pentacene, N,N' -diphenyl- N,N' -di(3-methylphenyl)-(1,1'-biphenyl)-4,4'-diamine (TPD) and tris(8-hydroquinolinato)aluminum (Alq_3) from ref. [36] are shown for comparison.

$50 \mu\text{W m}^{-1} \text{K}^{-2}$ was remarkably enhanced to $469 \mu\text{W m}^{-1} \text{K}^{-2}$.^[14] “Doping dilemma” inevitably obstructs the further enhancement of the figure of merit of conducting polymers. Therefore, it is important to systematically explore the doping effect on TE conversion in conducting polymers at the atomistic level. In the following, we will focus on how the doping affects the TE conversion in a p-type TE conducting polymer, PEDOT (Figure 5a). To fully take into account the doping effects, we herein for the first time explicitly incorporated the counter anion (Tos) (Figure 5b) and the ionized impurity scattering mechanism of charge carriers in our model. By the way, a recent theoretical work predicted that metal-coordination polymers, poly(Ni-ett) and its analogs can be high-performance “doping-free” TE materials, and chemical doping is not a must for such intrinsically conductive polymers, which might resolve the “doping dilemma” to some extent.^[61]

3.1.1. Doping-Induced Geometric and Electronic Structure Transition

The conjugated backbones of PEDOT showed an aromatic to quinoid-like structural transition after doping (Figure 5c), which

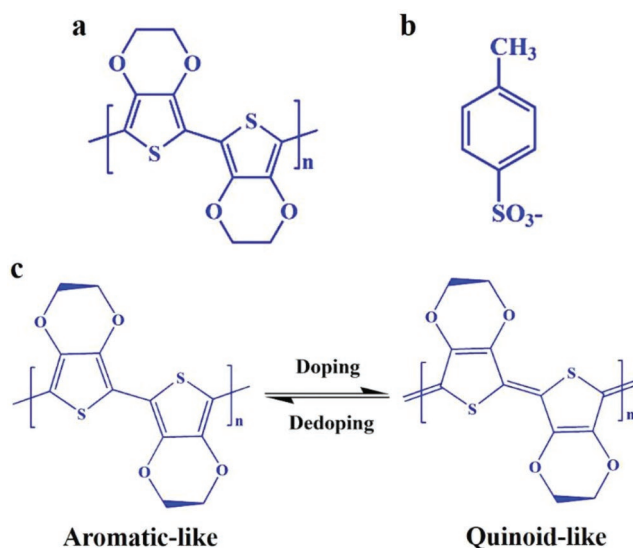


Figure 5. Chemical structures of a) PEDOT and b) Tos counter anion; c) PEDOT backbone conformation exhibiting an aromatic-to-quinone transition upon doping. All panels reproduced with permission.^[32] Copyright 2015, American Chemical Society.

is consistent with the previous theoretical result by Brédas and Kim;^[62] such backbone structural transition promotes the rigidity of polymer chains in the doped PEDOT:Tos. Moreover, the pristine PEDOT is a semiconductor, whereas both lightly and heavily doped crystalline PEDOT:Tos are metallic as the Fermi energy shifts into the valence band (VB) (Figure 6). The predicted metallic behavior for doped PEDOT:Tos agrees with the experimental reports based on the ultraviolet photoelectron spectroscopy, in which the researchers found π -electron signals at the Fermi level in PEDOT:Tos and PEDOT:PSS films.^[20a] The metallic band structure for doped PEDOT is also the origin of its high conductivity and metallic conductivity-temperature relation observed.^[20a] The hole concentration for the lightly and heavily doped crystalline PEDOT:Tos reaches 1.37×10^{20} and $5.77 \times 10^{20} \text{ cm}^{-3}$, respectively, and such level of hole concentration can be realized experimentally, such as in PEDOT:PSS films ($3 \times 10^{20} \text{ cm}^{-3}$)^[63] and PEDOT:Cl single crystals ($6.23 \times 10^{20} \text{ cm}^{-3}$).^[64] Furthermore, according to Bader’s charge analysis,^[65] each Tos is negatively charged with 0.89 and 0.87 electrons for the lightly and heavily doped crystalline PEDOT:Tos, respectively, while the PEDOT backbone is positively charged; the close-to-unity negative charge on Tos is in

Table 3. Optimal hole concentration, N_{opt} and peak value of figure of merit, zT_{max} for C_n -BTBTs at room temperature. Adapted with permission.^[31] Copyright 2014, American Chemical Society.

	Directions	S [$\mu\text{V K}^{-1}$]	σ [S cm^{-1}]	$S^2\sigma$ [$\mu\text{W m}^{-1} \text{K}^{-2}$]	κ_e [$\text{W m}^{-1} \text{K}^{-1}$]	zT_{max}	N_{opt} [10^{18} cm^{-3}]
C ₈ -BTBT	a	290	280	2.35×10^3	0.12	2.4	9.8
	b	290	257	2.10×10^3	0.10	2.2	9.8
C ₁₀ -BTBT	a	280	289	2.34×10^3	0.12	2.4	9.3
	b	280	259	2.02×10^3	0.11	2.1	9.3
C ₁₂ -BTBT	a	270	373	2.79×10^3	0.07	2.6	11
	b	270	293	2.10×10^3	0.12	1.8	9.3

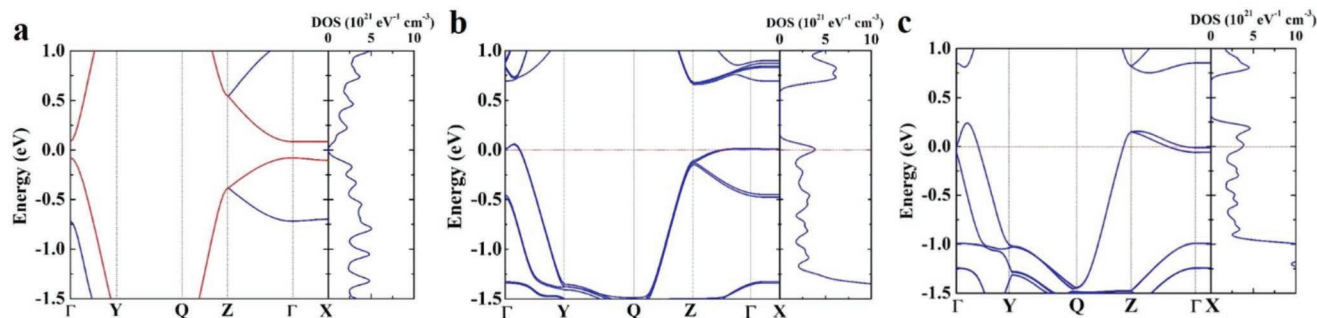


Figure 6. Band structures and DOS for a) pristine PEDOT, b) lightly doped PEDOT:Tos, and c) heavily doped PEDOT:Tos. The reciprocal coordinates of high-symmetry k -points in the first Brillouin zone are $\Gamma = (0, 0, 0)$, $Y = (0, 0.5, 0)$, $Q = (0, 0.5, 0.5)$, $Z = (0, 0, 0.5)$, and $X = (0.5, 0, 0)$, respectively. The Fermi level is shown with the red dashed line. All panels reproduced with permission.^[32] Copyright 2015, American Chemical Society.

agreement with the known fact that Tos is the counter anion in the polymerization of 3,4-ethylenedioxythiophene.

3.1.2. Doping Effect on Mobility and TE Conversion

As mentioned above, one of the long-standing difficulties we have been facing is the “doping dilemma” to enhance TE performance of conducting polymers. In the following, we will investigate the influence of doping on the charge transport and TE conversion of PEDOT. **Figure 7** shows the relationship between the TE transport coefficients and hole concentration for the

pristine crystalline PEDOT. Herein, only the acoustic phonon scattering is considered based on the DP approximation,^[25] and the rigid band approximation is utilized to mimic the doping effect. We find that with the hole concentration increasing, the conductivity increases linearly, while the Seebeck coefficient decreases dramatically (Figure 7a), and accordingly a maximum power factor is obtained at the optimal hole concentration (6.5×10^{19} and $7.7 \times 10^{19} \text{ cm}^{-3}$ for intrachain and interchain directions, respectively) (Figure 7b). Also, the electronic thermal conductivity increases linearly with the hole concentration (Figure 7c). As we know, in the free-electron gas model, the relationship between the electronic thermal conductivity and

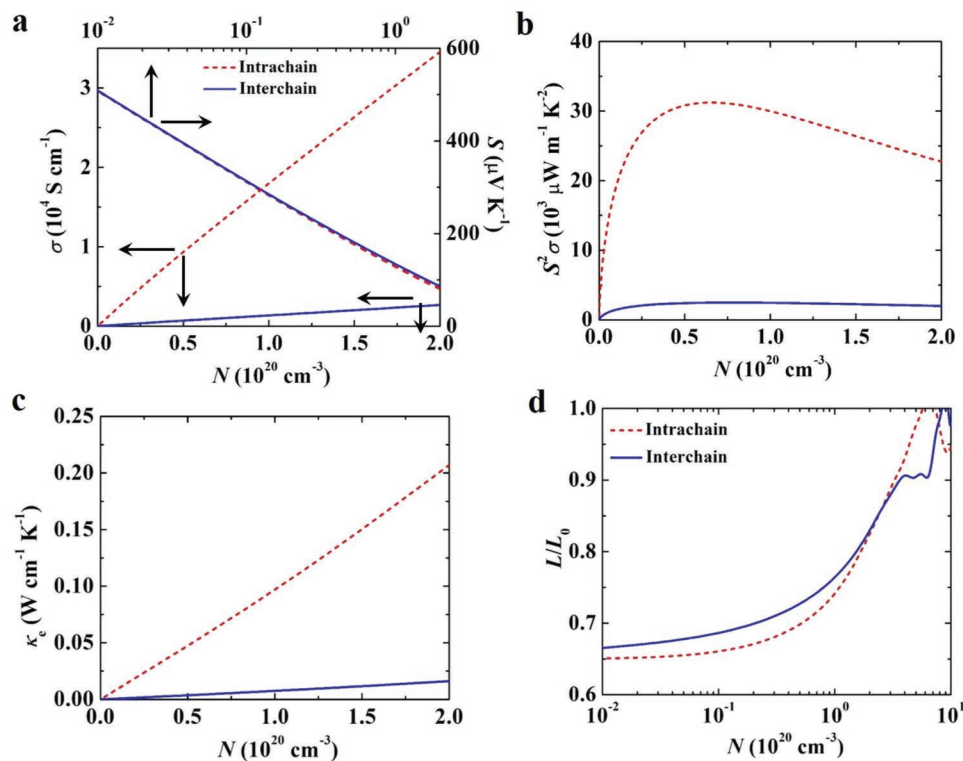


Figure 7. a) Conductivity, σ , Seebeck coefficient, S , b) power factor, $S^2\sigma$, c) electronic thermal conductivity, κ_e , and d) relative Lorenz number, L/L_0 varying with the hole concentration, N for the pristine PEDOT at room temperature. The intrachain and interchain directions represent the backbone and π - π stacking directions, respectively. All panels reproduced with permission.^[32] Copyright 2015, American Chemical Society.

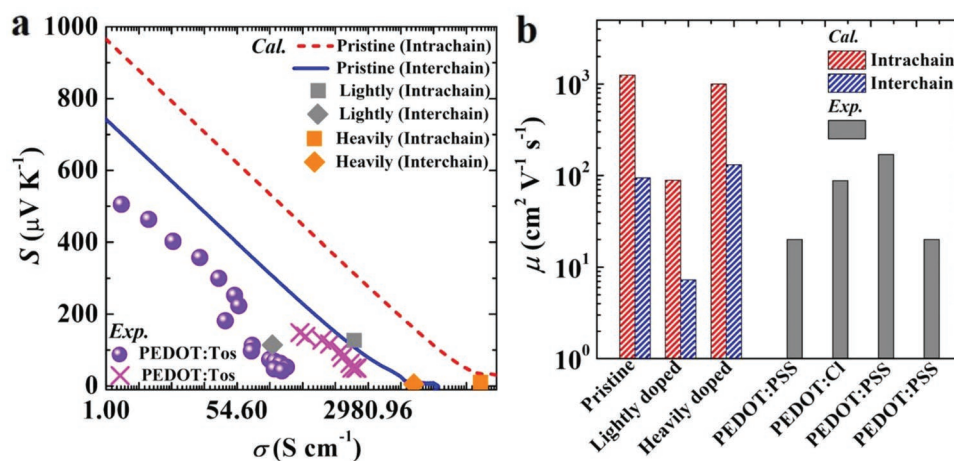


Figure 8. a) Relationship between Seebeck coefficient, S and conductivity, σ . The experimental data labeled by circles and crosses are taken from refs. [13] and [69] respectively. b) Predicted and measured mobility, μ for PEDOT. The experimental data (gray bars) from left to right are from refs. [70], [64], [71] and, [72] respectively. All panels reproduced with permission.^[32] Copyright 2015, American Chemical Society.

the conductivity satisfies the well-known Wiedemann–Franz law, $\kappa_e = L_0\sigma T$.^[66] At low hole concentrations in the pristine crystalline PEDOT, our calculated Lorentz number is smaller than the Sommerfeld value L_0 ; at high hole concentrations this value is close to the theoretical Sommerfeld value (Figure 7d). A recent experimental work by Cahill and co-workers indicated that the measured Lorenz number in PEDOT:PSS films is close to the Sommerfeld value.^[67] However, another measurement showed that the Lorenz number in PEDOT:Tos samples is larger than the Sommerfeld value, which has been ascribed to the bipolar contribution and phonon-assisted hopping in the disordered barrier regions.^[68]

To understand the relationship between the Seebeck coefficient and conductivity (Figure 8a), a simple analytic relation is derived by assuming the low hole concentration and the hole conduction in VB only as we have mentioned in Section 2.1^[40]

$$S = -\frac{k_B}{e} \ln \sigma + \frac{k_B}{e} \ln (N_{\text{eff}} e \mu) \quad (2)$$

The slope of the S - $\ln \sigma$ plot, that is, $-k_B/e \approx -86.17 \mu\text{V K}^{-1}$, depends on two physical constants (i.e., Boltzmann constant, k_B and elementary charge, e), and the intercept $(k_B/e) \ln (N_{\text{eff}} e \mu)$ is determined not only by the physical constants, but also by the intrinsic properties of a material (i.e., effective density of states, N_{eff} and the intrinsic mobility, μ). By analyzing the Seebeck coefficients and conductivities for PEDOT:Tos thin films measured by the accurate control of the oxidation level in ref. [13], a well-defined linear relationship with the slope of $-k_B/e$ has been identified (Figure 8a). In addition, the experimental data for PEDOT:Tos films measured through the electrochemical control of the oxidation level in ref. [69] also follow such linear trend (Figure 8a). However, all the experimental data plotted in Figure 8a are right below our predicted values, leading to the smaller intercept than our prediction. According to Equation (2), such deviation can be attributed to the overestimation of mobility arising from the neglect of explicit doping effect.

As we see above, Tos is negatively charged in the doped crystalline PEDOT:Tos, so when the holes on the PEDOT backbones

pass by these charged centers, their movement will be deflected due to the Coulomb attraction or repulsion between charged species. This is the so-called Coulomb scattering effect of charge carriers. Herein, we use Brooks–Herring approach to model the screened Coulomb scattering.^[73] The scattering rate is proportional to the ionized impurity concentration, which is 6.65×10^{20} and $1.39 \times 10^{21} \text{ cm}^{-3}$ for the lightly and heavily doped crystalline PEDOT:Tos. We find that the ionized impurity scattering plays a leading role over the acoustic phonon scattering spanning the temperature range of 10–300 K.^[32] Previous theoretical work has verified that the impurity scattering in silicon crystals is dominant at the carrier concentration higher than 10^{17} cm^{-3} .^[74] Besides, experimentalists have demonstrated that the mobility is governed by the ionized impurity scattering at the hole concentration of around 10^{20} cm^{-3} in PEDOT:Cl films.^[75]

The mobilities in the lightly doped crystalline PEDOT:Tos are 89.0 and $7.28 \text{ cm}^2 \text{V}^{-1} \text{s}^{-1}$ along the intrachain and interchain directions, respectively, while those in the heavily doped one are even larger (1000 and $131 \text{ cm}^2 \text{V}^{-1} \text{s}^{-1}$ along the intrachain and interchain directions, respectively) (Table 4), because the charge carrier concentration in the heavily doped crystalline PEDOT:Tos is higher ($5.77 \times 10^{20} \text{ cm}^{-3}$ vs $1.37 \times 10^{20} \text{ cm}^{-3}$), so that Coulomb screening effect is stronger and the scattering rate is lower. The similar trend was also observed in the experiments. Researchers even found that the field-effect hole mobility of poly(3-hexylthiophene) (P3HT) increased from around 3×10^{-5} to $6 \times 10^{-4} \text{ cm}^2 \text{V}^{-1} \text{s}^{-1}$ when the hole concentration increased from about 5×10^{16} to $8 \times 10^{19} \text{ cm}^{-3}$. Their explanation for the phenomenon is that holes can be easily trapped by energetic disorders or impurities at lower hole concentration, however, at higher hole concentration a portion of holes may fill all the traps, leading to the trap-free transport of the remaining holes.^[76]

Our estimated mobilities are in reasonable agreement with the recent experimental data (Figure 8b). Specifically, the single-crystal PEDOT:Cl nanowires were reported to possess a high mobility of $88.08 \text{ cm}^2 \text{V}^{-1} \text{s}^{-1}$ and conductivity of 8797 S cm^{-1} at the hole concentration of $6.23 \times 10^{20} \text{ cm}^{-3}$ along the π - π stacking direction,^[64] which are close to our prediction ($131 \text{ cm}^2 \text{V}^{-1} \text{s}^{-1}$ for mobility and $1.21 \times 10^4 \text{ S cm}^{-1}$ for conductivity at the hole

Table 4. TE properties of pristine PEDOT at the optimal hole concentration and two doped PEDOT:Tos. Available experimental results are shown for comparison. Reproduced with permission.^[32] Copyright 2015, American Chemical Society.

	Directions	Carrier concentration [10 ²⁰ cm ⁻³]	<i>S</i> [μV K ⁻¹]	σ [10 ³ S cm ⁻¹]	<i>S</i> ² σ [μW m ⁻¹ K ⁻²]	κ_e [W cm ⁻¹ K ⁻¹]	μ [cm ² V ⁻¹ s ⁻¹]	<i>L</i> / <i>L</i> ₀
Pristine	<i>b</i>	0.65	160	12.0	3.12 × 10 ⁴	0.06	1.25 × 10 ³	0.71
	<i>c</i>	0.77	150	1.05	2.48 × 10 ³	0.006	94.5	0.75
Lightly doped	<i>b</i>	1.37	130	1.95	3.15 × 10 ³	0.01	89.0	0.77
	<i>c</i>		110	0.16	209	0.0008	7.28	0.66
Heavily doped	<i>b</i>	5.77	10.0	92.6	921	0.68	1.00 × 10 ³	1.00
	<i>c</i>		5.00	12.1	310	0.08	131	0.93
PEDOT:Tos ^[13]			220	0.08	350			
PEDOT:PSS ^[14]			70.0	0.90	450			
PEDOT:Tos ^[69]			120	0.92	1.27 × 10 ³			

concentration of $5.77 \times 10^{20} \text{ cm}^{-3}$) for the heavily doped crystalline PEDOT:Tos in the same direction. Besides, the mobility shows highly anisotropic behavior—the intrachain mobility is ten times higher than the interchain one. Such anisotropy is also consistent with that reported for highly aligned nanocrystals of poly[4-(4,4-dihexadecyl-4H-cyclopenta[1,2-b:5,4-b']dithiophen-2-yl)-*alt*-[1,2,5]-thiadiazolo[3,4-*c*]pyridine] (PCDTPT) by Heeger and co-workers.^[77]

The power factor of lightly doped crystalline PEDOT:Tos is much higher than that of heavily doped one (Table 4), because the hole concentration in the former ($1.37 \times 10^{20} \text{ cm}^{-3}$) is closer to the predicted optimal carrier concentration (6.5×10^{19} and $7.7 \times 10^{19} \text{ cm}^{-3}$ for intrachain and interchain directions, respectively). Obviously, the heavily doped PEDOT:Tos here is over doped, even though the counterion concentration in the heavily doped PEDOT:Tos only doubles comparing to lightly doped one, which hints that precisely tuning the carrier concentration via chemical doping toward enhanced TE efficiency will be very challenging and a delicate task. We noted that the predicted power factors of lightly doped crystalline PEDOT:Tos (3150 and 209 $\mu\text{W m}^{-1} \text{ K}^{-2}$ along the intrachain and interchain directions, respectively) are very close to the experimental results of 1270 $\mu\text{W m}^{-1} \text{ K}^{-2}$ reported in ref. [69] and 350 $\mu\text{W m}^{-1} \text{ K}^{-2}$ in ref. [13].

3.2. Intrachain versus Interchain TE Transport in PEDOT:Tos

Usually, polymers are regarded as thermal insulators with ultralow lattice thermal conductivity ($\approx 0.1\text{--}1 \text{ W m}^{-1} \text{ K}^{-1}$). Whereas, more and more experimental and theoretical studies have proven that the lattice thermal conductivity of polymers are not intrinsically low, instead it can be astonishingly high.^[78] We first extracted the intrachain and interchain lattice thermal conductivities for both pristine and lightly doped crystalline PEDOT:Tos based on classical NEMD simulations (Table 5).^[79] Our results clearly show the thermal conductor character of PEDOT with very high lattice thermal conductivity in the backbone direction (41.7 and 61.2 $\text{W m}^{-1} \text{ K}^{-1}$ for pristine and lightly doped PEDOT, respectively), however the thermal insulator behavior with much lower lattice thermal conductivity

in the π - π stacking direction (0.33 and 0.14 $\text{W m}^{-1} \text{ K}^{-1}$ for pristine and lightly doped PEDOT, respectively), which amounts to more than 100-fold anisotropy. We noted that the 180-fold anisotropy for the lattice thermal conductivity between the intrachain and interchain directions was reported in the previous experimental work for the highly oriented polyethylene (PE) fibers.^[80]

The vast anisotropy for lattice thermal transport in crystalline polymers originates from the distinct bonding natures in two directions—strong covalent bonds in the backbone direction versus weak van der Waals forces in the π - π stacking direction. Figure 9 shows that the room-temperature intrachain lattice thermal conductivities of highly aligned polymers are around 10–100 $\text{W m}^{-1} \text{ K}^{-1}$, while those in the perpendicular directions fall into the range of 0.1–1 $\text{W m}^{-1} \text{ K}^{-1}$. For example, it was recently reported that the crystalline PE nanofibers possessed a superb intrachain lattice thermal conductivity of 50 $\text{W m}^{-1} \text{ K}^{-1}$.^[86] The lattice thermal conductivity in the high-quality ultradrawn PE single-crystalline nanofibers can reach as high as 104 $\text{W m}^{-1} \text{ K}^{-1}$, even higher than plenty of metals.^[83] In contrast, the amorphous polymers show room-temperature lattice thermal conductivities within 0.1–1 $\text{W m}^{-1} \text{ K}^{-1}$ owing to their disordered structures. For instance, the thermal conductivity of amorphous PEDOT:PSS and PEDOT:Tos films was reported to be 0.42^[14] and 0.37 $\text{W m}^{-1} \text{ K}^{-1}$,^[13] respectively.

As illustrated by the kinetic theory of gas (i.e., $\kappa_L = c_V v^2 \tau$), the lattice thermal conductivity depends on the specific heat capacity, c_V , the phonon group velocity, v , as well as the phonon relaxation time, τ . Herein, the phonon group velocity is determined by the elastic constant, C , and the mass density, ρ , according to the relation $v = \sqrt{C/\rho}$; the phonon relaxation time is related

Table 5. Elastic constant, C , phonon group velocity, v , phonon mean free paths, l_{phonon} , phonon relaxation time, τ , lattice thermal conductivity, κ_L , and hole mean free path, l_{hole} for the pristine PEDOT and lightly doped PEDOT:Tos, respectively at room temperature. Adapted with permission.^[79] Copyright 2017, Wiley.

	Directions	C [10 ⁹ m ⁻³]	v [10 ³ m s ⁻¹]	l_{phonon}	τ [ps]	κ_L [W m ⁻¹ K ⁻¹]	l_{hole} [Å]
Pristine	<i>b</i> *	232	11.8	479	4.06	41.7	13.2
	<i>c</i> *	19.0	3.36	25.0	0.74	0.33	4.17
Lightly doped	<i>b</i> *	195	11.6	1.11 × 10 ³	9.57	61.2	4.04
	<i>c</i> *	46.3	5.65	17.8	0.32	0.14	1.24

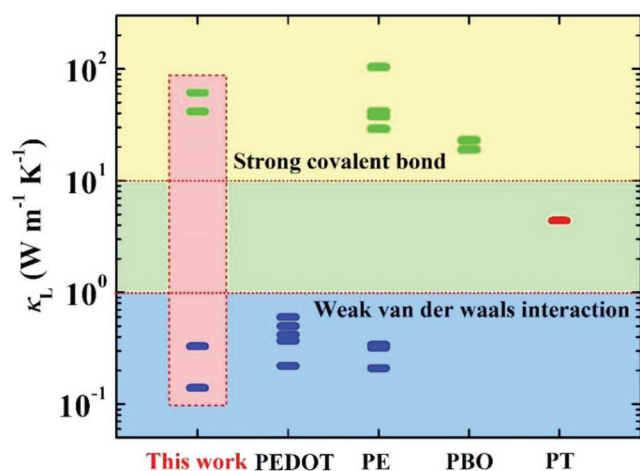


Figure 9. Room-temperature intrachain (the green bar) and interchain (the blue bar) lattice thermal conductivities, κ_L for the pristine PEDOT and lightly doped PEDOT:Tos (in the shaded red box). The experimental data are shown for comparison, with references collected in Table 6. Reproduced with permission.^[79] Copyright 2017, Wiley.

to the phonon mean free path, l , and the group velocity, v by $\tau = l/v$. We find that the elastic constant shows distinct anisotropy (190×10^9 and 232×10^9 J m⁻³ for pristine and doped PEDOT in the backbone direction; 19×10^9 and 46×10^9 J m⁻³ in the stacking direction), and our elastic constant in the chain direction is on the same order of magnitude as the one measured for the crystalline PE nanofibers ($\approx 300 \times 10^9$ J m⁻³).^[87] The phonon mean free path is also distinctly anisotropic (479 and 1100 Å for pristine and doped PEDOT in the backbone direction; 25.0 and 17.8 Å in the stacking direction). The predicted intrachain mean free path of phonons is close to the one measured for the crystalline polybenzobisoxazole (PBO) fiber (≈ 300 Å).^[84] Based on the discussions above, we conclude that

Table 6. Sources of experimental lattice thermal conductivity, κ_L shown in Figure 9. Adapted with permission.^[79] Copyright 2017, Wiley.

	κ_L [W m ⁻¹ K ⁻¹]	References
PEDOT:Tos films	<0.37 (lateral)	[13]
	0.5 (in-plane)	[68]
PEDOT:PSS films	<0.42 (in-plane)	[14]
	0.6 (in-plane)	[67]
	0.22 (in-plane)	[81]
PE fibers	37.5 (parallel to fiber)	[80]
	0.21 (perpendicular to fiber)	
PE single crystal	41.6 (axial)	[82]
	0.34 (transverse)	
PE gel	29.1 (axial)	
	0.321 (transverse)	
PE nanofibers	104 (along fiber axis)	[83]
PBO fibers	19 (along fiber axis)	[84]
	23 (along fiber axis)	
Polythiophene chain-oriented amorphous nanofibers	4.4 (along fiber axis)	[85]

the anisotropy of lattice thermal conductivity in crystalline conducting polymers originates from the anisotropy of phonon group velocity and phonon mean free path.

As demonstrated, the crystalline conducting polymers are “electron-crystal, phonon-glass” because they possess excellent intrachain charge transport property and poor interchain thermal transport property, but unfortunately they are electron-crystal in one direction and phonon-glass in the other direction. One serious problem we face is that despite the high intrachain power factor as seen in Section 3.1.2, the intrachain figure of merit (0.02) is much lower than the interchain one (0.19), because of more than 100-fold anisotropy of lattice thermal conductivities and tenfold anisotropy of power factors (Figure 10a). To fully utilize the high intrachain power factor of conducting polymers, we are motivated to suppress the intrachain lattice thermal conductivity. In the next section, we will focus on tuning the intrachain lattice thermal conductivity via regulation of the polymer chain length and introducing local structural disorders.

3.3. Tuning Chain Length and Crystallinity toward Enhanced Figure of Merit

First, we will discuss how the polymer chain length affects the intrachain lattice thermal conductivity and figure of merit. Our hypothesis is based on that the hole and phonon mean free paths can be separated in length scales, so we can synthesize chain-oriented polymer fibers in which the polymer chain is longer than the mean free path of hole but shorter than that of phonon (Figure 10b). By doing so, the lattice thermal conductivity can be dramatically suppressed owing to the boundary scattering effect, yet the hole mobility and power factor would not be affected (Figure 10c). To verify our hypothesis, we compared the estimated intrachain hole and phonon mean free paths (Table 5), and found that the hole mean free path (13.2 and 4.04 Å for pristine and lightly doped crystalline PEDOT, respectively) is indeed more than ten times shorter than the phonon mean free path (479 and 1000 Å for pristine and lightly doped crystalline PEDOT, respectively). The separation of distances that hole and phonon travel along the polymer chain guarantees that regulation of the polymer chain length can suppress the phonon transport but not affect the hole transport along the chain direction.

Guided by the above-mentioned design principle, the chain length of PEDOT should be longer than 13.2 Å while shorter than 479 Å, amounting to 4–124 EDOT units and relative molecular weight (rmw) of 560–17 360. Here, two representative polymers, **Polymer 1** and **Polymer 2**, have been designed. Their chain length is 156 and 391 Å, and rmw is 5600 and 14 000, containing 40 and 100 EDOT moieties, respectively. The lattice thermal conductivity is 4.84 W m⁻¹ K⁻¹ for **Polymer 1** and it is 9.84 W m⁻¹ K⁻¹ for **Polymer 2**, nine and four times, respectively, lower than the value predicted for “ideal” crystalline PEDOT. Accordingly, the intrachain figure of merit is enhanced to 0.16 and 0.09, respectively. As demonstrated, tuning the polymer chain length is an effective strategy for suppression of lattice thermal conductivity and enhancement of figure of merit.

Then a question arises: Can the intrachain lattice thermal conductivity be further suppressed for even higher figure of merit? One thing to keep in mind is that **Polymers 1** and **2** designed

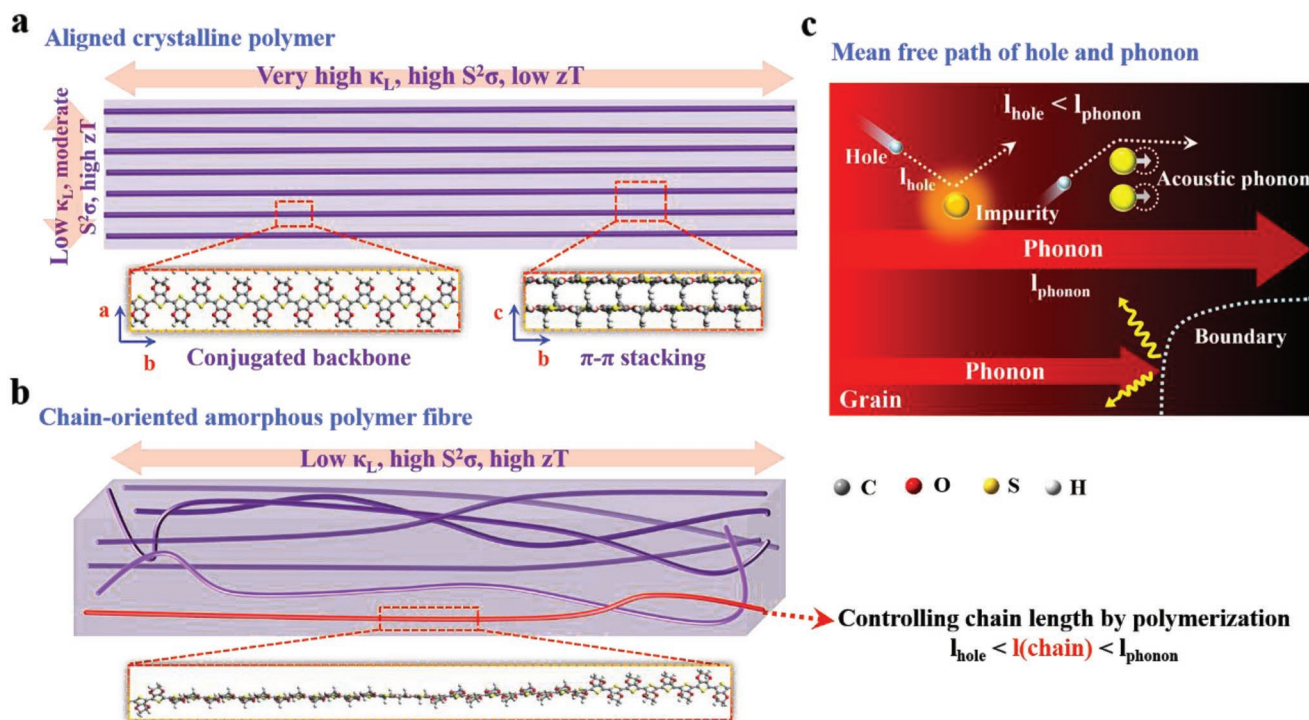


Figure 10. a) Intrachain and interchain TE transport properties of the crystalline polymeric materials. b) Suppression of the thermal transport in the chain-oriented amorphous polymer fibers. The chain length is tailored to be shorter than the phonon mean free path while longer than the hole mean free path. c) Separation of the length scales for the thermal and hole transport in the same crystallite. In general, the mean free path of phonons is much longer than that of holes; therefore, the phonons will be mainly scattered by the grain boundary, if the grain size is smaller than the phonon mean free path. All panels reproduced with permission.^[79] Copyright 2017, Wiley.

above are highly ordered crystals. Previous experimental work by Chen and co-workers has revealed that the chain entanglements, voids, and defects in polymeric materials can introduce extra scattering events and reduce the lattice thermal conductivity.^[83] To answer the question, on the basis of **Polymers 1** and **2**, a series of chain-oriented fibers with various degrees of structural order were prepared using the simulated annealing approach. The structural order of polymer fibers is characterized by the volume crystallinity, X_c , defined as $X_c = (\rho - \rho_a)/(\rho_c - \rho_a)$, where ρ is the sample density; ρ_c ($= 1.68 \text{ g cm}^{-3}$) and ρ_a ($= 1.00 \text{ g cm}^{-3}$)

are the densities of crystalline and amorphous samples, respectively. The crystallinity of 20 fibers prepared based on **Polymer 1** and 18 fibers based on **Polymer 2** spans the range of 0.49–0.87 and 0.54–0.89, respectively.

Figure 11a shows that with the decreased crystallinity, the lattice thermal conductivity is suppressed significantly from 4.88 to 0.97 $\text{W m}^{-1} \text{K}^{-1}$ for **Polymer 1**, and it is dramatically reduced from 6.66 to 1.67 $\text{W m}^{-1} \text{K}^{-1}$ for **Polymer 2**. Compared with the lattice thermal conductivity of “ideal” crystalline PEDOT (41.7 $\text{W m}^{-1} \text{K}^{-1}$), the thermal conductivities of chain-oriented

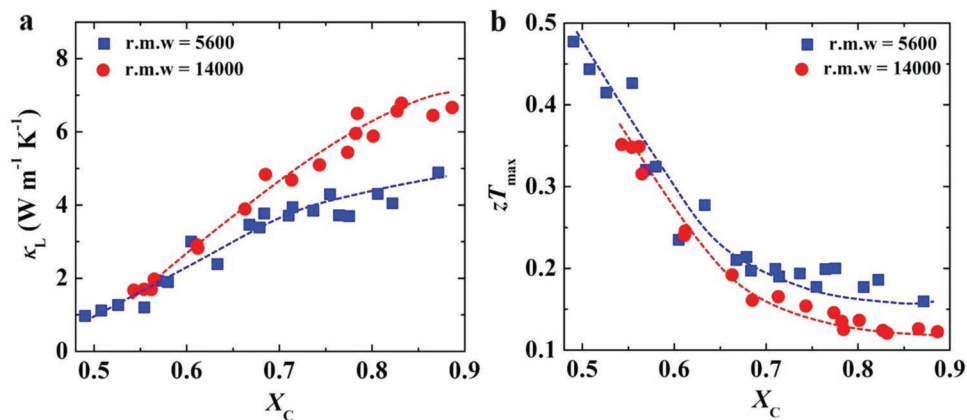


Figure 11. Dependence of a) the intrachain lattice thermal conductivity, κ_L , and b) maximum figure of merit, zT_{max} on the crystallinity, X_c of chain-oriented PEDOT fibers at room temperature. The dashed lines are displayed for the eye guide. All panels reproduced with permission.^[79] Copyright 2017, Wiley.

fibers are ten times lower. Very recently, experimentalists utilized electrostatic repulsive forces to stretch the polyacrylic acid backbone at the molecular level, resulting in extended backbone conformations, well-packed chains, and thereby lattice thermal conductivities significantly enhanced from 0.34 to $1.2 \text{ W m}^{-1} \text{ K}^{-1}$ at room temperature,^[88] suggesting that it is quite feasible to tune the lattice thermal conductivity of polymeric materials through the morphology control.

It is intriguing to find that the intrachain figure of merit for **Polymer 1** with the crystallinity of 0.49 has been enhanced to 0.48 by the rational control of structural disorder (Figure 11b), 24 times higher than that for the original “ideal” crystal (0.02). Such high room-temperature p-type figure of merit is close to the current record-high values for PEDOT-based TE materials obtained in experiments, such as zT of 0.42 in PEDOT:PSS films by Pipe and co-workers,^[14] zT of 0.25 in PEDOT:Tos films by Crispin and co-workers,^[13] and zT of 0.58 in PEDOT/ Bi_2Te_3 hybrid films by Wang et al.^[89] Our results show that suppressing the thermal transport provides a new route for achieving high figure of merit in conducting polymers.

4. Conclusions and Outlook

In conclusion, first-principles-guided design of organic TE materials plays an indispensable role nowadays, since it can provide insightful understandings of the microscopic physical process, and easily build the fundamental structure–property relation, which will speed up the discovery of high-performance organic TE materials. Over the past ten years, we have been devoted to developing a parameter-free computational scheme^[27] to predict the TE figure of merit of organic materials. As manifested by the experimental verification of the predicted mobility and Seebeck coefficient for C_n -BTBTs, the computational methods are reliable and so far state-of-the-art. With the help of this computational scheme, we also take one step forward to explore the rational design strategy for high-performance organic TE materials, covering both small-molecule organic semiconductors and conducting polymers. We have reached the following conclusions:

- (i) In view of the negative effect of molecular dopants on the charge transport, we propose to search for high-performance small-molecule organic TE materials in the category of high intrinsic mobility. More importantly, introducing long alkyl side chains to conjugated backbones may enhance the TE performance. Such as in C_n -BTBTs, the hole mobilities increase with the length of alkyl chains due to the closer packing of conjugated backbones; and on the other hand, thanks to plenty of low-frequency phonon modes introduced by the long alkyl side chains, the lattice thermal conductivity is suppressed to an extremely low level.
- (ii) Taking the example of conducting polymer PEDOT, we uncover the “doping dilemma” in the TE conversion. We find that the chemical doping not only changes geometric and electronic structure of host polymers, but also introduces additional scattering centers of charge carriers. The ionized impurity scattering arising from the counter anions plays a

dominant role in the charge transport of doped PEDOT:Tos at the hole concentration of 1.37×10^{20} and $5.77 \times 10^{20} \text{ cm}^{-3}$. The calculated Seebeck coefficient, mobility, and power factor for the doped PEDOT:Tos are comparable to the experimental results. The TE properties of lightly doped PEDOT:Tos are superior to those of heavily doped one, because its carrier concentration is closer to the optimal doping level.

- (iii) The crystalline PEDOT exhibits quite high intrachain ($\approx 50 \text{ W m}^{-1} \text{ K}^{-1}$) but very low interchain lattice thermal conductivity ($< 0.5 \text{ W m}^{-1} \text{ K}^{-1}$), stemming from the different chemical bonds in the two directions, that is, strong covalent bonds versus weak van der Waals forces. Therefore, the intrachain figure of merit of crystalline PEDOT is inevitably low; even the power factor in this direction is ten times higher.
- (iv) We propose that regulation of the chain length and tuning the degree of structural disorder are two effective strategies to suppress the intrachain lattice thermal conductivity. And by engineering the crystallinity and chain length, a significant improvement of intrachain figure of merit (≈ 0.48) has been realized, which is 24 times higher than the original crystalline samples.

Despite the computational progress made toward understanding the TE conversion in organic materials, more elaborate theoretical models and accurate computational methods are under development in order to fully understand more experimental outcomes and the underlying rules governing the TE conversion of organic TE materials.

- (i) Density functional perturbation theory (DFPT)^[90] combined with Wannier function-based interpolation technique^[91] is a powerful tool to estimate the electron–phonon scattering quantitatively. Unfortunately, it is still demanding to widely apply this approach for the organic condensed matter due to the high computational costs. So far, we have only employed this scheme in some low-dimensional systems, such as graphene,^[92] graphyne,^[93] stanene,^[94] and GeAs_2 .^[95] Only a few pioneering works adopted this method to evaluate the electron–phonon scattering in organic model systems, such as in naphthalene crystal,^[96] K_3 picene crystal,^[97] and isolated poly(Ni-ett) chain.^[41] Very recently, a new approach, the electron–phonon averaged approximation that combines simplicity and speed with a fully first-principles treatment of the electron–phonon coupling has been developed.^[98] We believe that this methodology advancement will facilitate the fundamental insight of TE transport process in organic materials in the near future.
- (ii) We utilize an “ideal” crystal model representing the crystalline regions of real materials and assume that the charge transport can be described by the delocalized band picture.^[99] Whereas, in real organic solids, especially in polymers, due to the weak intermolecular interactions the structural disorders arise, which leads to charge carrier localizations, and in such case the band picture is no longer valid.^[100] It is thereby of great interest to develop hopping transport models to study the TE properties in organic disordered materials at the first-principles level. Very recently,

Tessler and Mendels,^[101] Zozoulenko and co-workers,^[102] and Lu et al.^[103] have successively investigated the TE properties of disordered organic semiconductors under the premise of Gaussian disorder model, in which the probability of hopping between two sites adopts Miller–Abraham’s or Marcus formula. This model depends on several physical quantities, such as the broadening of Gaussian function, the localization length, the transfer integral, etc., which are taken as empirical parameters. To the best of our knowledge, the combination of first-principles determination of these parameters with the hopping transport model of charge carriers is still lacking.

(iii) Extraordinary progress has recently been achieved in the composite TE materials,^[104] especially in the polymer–inorganic hybrid materials.^[15] The reported room-temperature figure of merit of 0.5 for n-type hybrids of carbon nanotubes and PEDOT films treated by tetrakis(dimethylamino)ethylene has exceeded the pure organic TE materials.^[106] Furthermore, an ultrahigh p-type figure of merit of 0.58 has been realized in PEDOT/Bi₂Te₃ hybrid films at room temperature.^[89] Extremely high conductivity ($1.9 \times 10^5 \text{ S m}^{-1}$) and the record-high power factor ($2710 \mu\text{W m}^{-1} \text{ K}^{-2}$) have been achieved in completely carbon-based composite materials comprised of polyaniline, graphene, PEDOT:PSS, and double-walled nanotube.^[107] Hence, it is very interesting to systematically study the hybrid TE materials. However, as far as we know, theoretical investigations on the organic–inorganic hybrid TE materials are rare. Preliminary study of the TE properties of organic–inorganic hybrid perovskite (CH₃NH₃PbI₃) has been conducted by our group.^[33,108]

We anticipate that this review will not only be of assistance to the experimentalists in developing high-efficiency organic TE materials, but also motivate more and more fundamental theoretical researches on the improvement of computational methods used in this field for the next decades.

Acknowledgements

This work was supported by the National Natural Science Foundation of China (Grant Nos. 21673123 and 21788102) and the Ministry of Science and Technology of China (Grant No. 2017YFA0204501). Computational resources were provided by the Tsinghua Supercomputing Center.

Conflict of Interest

The authors declare no conflict of interest.

Keywords

figure of merit, first-principles calculations, organic thermoelectric materials

Received: December 3, 2018
Revised: January 7, 2019
Published online:

- [1] J. He, T. M. Tritt, *Science* **2017**, *357*, eaak9997.
[2] L. E. Bell, *Science* **2008**, *321*, 1457.
[3] A. F. Joffe, L. S. Stilbans, *Rep. Prog. Phys.* **1959**, *22*, 167.
[4] D. M. Rowe, *CRC Handbook of Thermoelectrics*, CRC Press, Boca Raton, FL **1995**.
[5] F. J. Disalvo, *Science* **1999**, *285*, 703.
[6] G. J. Snyder, E. S. Toberer, *Nat. Mater.* **2008**, *7*, 105.
[7] a) H. J. Goldsmid, *Proc. Phys. Soc.* **1958**, *71*, 633; b) B. Poudel, Q. Hao, Y. Ma, Y. Lan, A. Minnich, B. Yu, X. Yan, D. Wang, A. Muto, D. Vashaee, X. Chen, J. Liu, M. S. Dresselhaus, G. Chen, Z. Ren, *Science* **2008**, *320*, 634; c) R. Venkatasubramanian, E. Siivola, T. Colpitts, B. O’quinn, *Nature* **2001**, *413*, 597.
[8] T. A. Skotheim, J. Reynolds, *Handbook of Conducting Polymers*, CRC Press, Boca Raton, FL **2007**.
[9] Y. Chen, Y. Zhao, Z. Liang, *Energy Environ. Sci.* **2015**, *8*, 401.
[10] B. Russ, A. Glaudell, J. J. Urban, M. L. Chabiny, R. A. Segalman, *Nat. Rev. Mater.* **2016**, *1*, 16050.
[11] a) O. Bubnova, X. Crispin, *Energy Environ. Sci.* **2012**, *5*, 9345; b) M. He, F. Qiu, Z. Lin, *Energy Environ. Sci.* **2013**, *6*, 1352; c) T. O. Poehler, H. E. Katz, *Energy Environ. Sci.* **2012**, *5*, 8110; d) R. Kroon, D. A. Mengistie, D. Kiefer, J. Hynynen, J. D. Ryan, L. Yu, C. Müller, *Chem. Soc. Rev.* **2016**, *45*, 6147.
[12] Z. U. Khan, J. Edberg, M. M. Hamed, R. Gabrielsson, H. Granberg, L. Wågberg, I. Engquist, M. Berggren, X. Crispin, *Adv. Mater.* **2016**, *28*, 4556.
[13] O. Bubnova, Z. U. Khan, A. Malti, S. Braun, M. Fahlman, M. Berggren, X. Crispin, *Nat. Mater.* **2011**, *10*, 429.
[14] G. H. Kim, L. Shao, K. Zhang, K. P. Pipe, *Nat. Mater.* **2013**, *12*, 719.
[15] a) Q. Zhang, Y. Sun, W. Xu, D. Zhu, *Adv. Mater.* **2014**, *26*, 6829; b) R. M. W. Wolfe, A. K. Menon, T. R. Fletcher, S. R. Marder, J. R. Reynolds, S. K. Yee, *Adv. Funct. Mater.* **2018**, *28*, 1803275; c) A. K. Menon, R. M. W. Wolfe, S. R. Marder, J. R. Reynolds, S. K. Yee, *Adv. Funct. Mater.* **2018**, *28*, 1801620; d) W. Jin, L. Liu, T. Yang, H. Shen, J. Zhu, W. Xu, S. Li, Q. Li, L. Chi, C.-A. Di, D. Zhu, *Nat. Commun.* **2018**, *9*, 3586.
[16] Y. Sun, L. Qiu, L. Tang, H. Geng, H. Wang, F. Zhang, D. Huang, W. Xu, P. Yue, Y.-S. Guan, F. Jiao, Y. Sun, D. Tang, C.-A. Di, Y. Yi, D. Zhu, *Adv. Mater.* **2016**, *28*, 3351.
[17] Y. Sun, P. Sheng, C. Di, F. Jiao, W. Xu, D. Qiu, D. Zhu, *Adv. Mater.* **2012**, *24*, 932.
[18] a) O. Bubnova, M. Berggren, X. Crispin, *J. Am. Chem. Soc.* **2012**, *134*, 16456; b) S. Wang, H. Sun, U. Ail, M. Vagin, P. O. Å. Persson, J. W. Andreasen, W. Thiel, M. Berggren, X. Crispin, D. Fazzi, S. Fabiano, *Adv. Mater.* **2016**, *28*, 10764; c) D. Huang, C. Wang, Y. Zou, X. Shen, Y. Zang, H. Shen, X. Gao, Y. Yi, W. Xu, C.-A. Di, D. Zhu, *Angew. Chem., Int. Ed.* **2016**, *55*, 10672; d) Q. Zhang, Y. Sun, W. Xu, D. Zhu, *Energy Environ. Sci.* **2012**, *5*, 9639; e) H. Park, S. H. Lee, F. S. Kim, H. H. Choi, I. W. Cheong, J. H. Kim, *J. Mater. Chem. A* **2014**, *2*, 6532; f) A. M. Glaudell, J. E. Cochran, S. N. Patel, M. L. Chabiny, *Adv. Energy Mater.* **2015**, *5*, 1401072.
[19] K. P. Pernstich, B. Rossner, B. Batlogg, *Nat. Mater.* **2008**, *7*, 321.
[20] a) O. Bubnova, Z. U. Khan, H. Wang, S. Braun, D. R. Evans, M. Fabretto, P. Hojati-Talemi, D. Dagnelund, J.-B. Arlin, Y. H. Geerts, S. Desbief, D. W. Breiby, J. W. Andreasen, R. Lazzaroni, W. M. Chen, I. Zozoulenko, M. Fahlman, P. J. Murphy, M. Berggren, X. Crispin, *Nat. Mater.* **2014**, *13*, 190; b) Z. Fan, P. Li, D. Du, J. Ouyang, *Adv. Energy Mater.* **2017**, *7*, 1602116; c) S. N. Patel, A. M. Glaudell, K. A. Peterson, E. M. Thomas, K. A. O’hara, E. Lim, M. L. Chabiny, *Sci. Adv.* **2017**, *3*, e1700434.
[21] a) D. Huang, H. Yao, Y. Cui, Y. Zou, F. Zhang, C. Wang, H. Shen, W. Jin, J. Zhu, Y. Diao, W. Xu, C.-A. Di, D. Zhu, *J. Am. Chem. Soc.* **2017**, *139*, 13013; b) K. Shi, F. Zhang, C.-A. Di, T.-W. Yan, Y. Zou, X. Zhou, D. Zhu, J.-Y. Wang, J. Pei, *J. Am. Chem.*

- Soc.* **2015**, 137, 6979; c) B. Russ, M. J. Robb, F. G. Brunetti, P. L. Miller, E. E. Perry, S. N. Patel, V. Ho, W. B. Chang, J. J. Urban, M. L. Chabinyk, C. J. Hawker, R. A. Segalman, *Adv. Mater.* **2014**, 26, 3473; d) C.-K. Mai, R. A. Schlitz, G. M. Su, D. Spitzer, X. Wang, S. L. Fronk, D. G. Cahill, M. L. Chabinyk, G. C. Bazan, *J. Am. Chem. Soc.* **2014**, 136, 13478; e) H. Li, M. E. Decoster, R. M. Ireland, J. Song, P. E. Hopkins, H. E. Katz, *J. Am. Chem. Soc.* **2017**, 139, 11149.
- [22] M. Culebras, C. M. Gomez, A. Cantarero, *J. Mater. Chem. A* **2014**, 2, 10109.
- [23] J. Chen, D. Wang, Z. Shuai, *J. Chem. Theory Comput.* **2012**, 8, 3338.
- [24] J. M. Ziman, *Principles of the Theory of Solids*, Cambridge University Press, Cambridge **1971**.
- [25] J. Bardeen, W. Shockley, *Phys. Rev.* **1950**, 80, 72.
- [26] Z. Shuai, D. Wang, Q. Peng, H. Geng, *Acc. Chem. Res.* **2014**, 47, 3301.
- [27] D. Wang, W. Shi, J. Chen, J. Xi, Z. Shuai, *Phys. Chem. Chem. Phys.* **2012**, 14, 16505.
- [28] a) M.-Q. Long, L. Tang, D. Wang, L. Wang, Z. Shuai, *J. Am. Chem. Soc.* **2009**, 131, 17728; b) M. Long, L. Tang, D. Wang, Y. Li, Z. Shuai, *ACS Nano* **2011**, 5, 2593.
- [29] a) J. Chen, J. Xi, D. Wang, Z. Shuai, *J. Phys. Chem. Lett.* **2013**, 4, 1443; b) J. Xi, M. Long, L. Tang, D. Wang, Z. Shuai, *Nanoscale* **2012**, 4, 4348.
- [30] L. Tang, M. Long, D. Wang, Z. Shuai, *Sci. China, Ser. B: Chem.* **2009**, 52, 1646.
- [31] W. Shi, J. Chen, J. Xi, D. Wang, Z. Shuai, *Chem. Mater.* **2014**, 26, 2669.
- [32] W. Shi, T. Zhao, J. Xi, D. Wang, Z. Shuai, *J. Am. Chem. Soc.* **2015**, 137, 12929.
- [33] T. Zhao, W. Shi, J. Xi, D. Wang, Z. Shuai, *Sci. Rep.* **2016**, 7, 19968.
- [34] a) X. Yong, W. Shi, G. Wu, S. S. Goh, S. Bai, J.-W. Xu, J.-S. Wang, S.-W. Yang, *J. Mater. Chem. A* **2018**, 6, 19757; b) J. Khan, Y. Liu, T. Zhao, H. Geng, W. Xu, Z. Shuai, *J. Comput. Chem.* **2018**, 39, 2582.
- [35] D. Wang, L. Tang, M. Long, Z. Shuai, *J. Phys. Chem. C* **2011**, 115, 5940.
- [36] N. Kim, B. Domercq, S. Yoo, A. Christensen, B. Kippelen, S. Graham, *Appl. Phys. Lett.* **2005**, 87, 241908.
- [37] M. Uno, I. Doi, K. Takimiya, J. Takeya, *MRS Proc.* **2011**, B10, 1154.
- [38] D. Wang, L. Tang, M. Long, Z. Shuai, *J. Chem. Phys.* **2009**, 131, 224704.
- [39] K. Harada, M. Sumino, C. Adachi, S. Tanaka, K. Miyazaki, *Appl. Phys. Lett.* **2010**, 96, 253304.
- [40] H. Fritzsche, *Solid State Commun.* **1971**, 9, 1813.
- [41] W. Shi, G. Wu, X. Yong, T. Deng, J.-S. Wang, J.-C. Zheng, J. Xu, M. B. Sullivan, S.-W. Yang, *ACS Appl. Mater. Interfaces* **2018**, 10, 35306.
- [42] K. Takimiya, S. Shinamura, I. Osaka, E. Miyazaki, *Adv. Mater.* **2011**, 23, 4347.
- [43] H. Minemawari, T. Yamada, H. Matsui, J. Y. Tsutsumi, S. Haas, R. Chiba, R. Kumai, T. Hasegawa, *Nature* **2011**, 475, 364.
- [44] Y. Yuan, G. Giri, A. L. Ayzner, A. P. Zoombelt, S. C. B. Mannsfeld, J. Chen, D. Nordlund, M. F. Toney, J. Huang, Z. Bao, *Nat. Commun.* **2014**, 5, 3005.
- [45] C. Liu, T. Minari, X. Lu, A. Kumatani, K. Takimiya, K. Tsukagoshi, *Adv. Mater.* **2011**, 23, 523.
- [46] D. He, J. Qiao, L. Zhang, J. Wang, T. Lan, J. Qian, Y. Li, Y. Shi, Y. Chai, W. Lan, L. K. Ono, Y. Qi, J.-B. Xu, W. Ji, X. Wang, *Sci. Adv.* **2017**, 3, e1701186.
- [47] T. R. Arend, A. Wimmer, G. Schweicher, B. Chattopadhyay, Y. H. Geerts, R. Kersting, *J. Phys. Chem. Lett.* **2017**, 8, 5444.
- [48] J. P. Perdew, K. Burke, M. Ernzerhof, *Phys. Rev. Lett.* **1996**, 77, 3865.
- [49] S. Grimme, *J. Comput. Chem.* **2006**, 27, 1787.
- [50] T. Izawa, E. Miyazaki, K. Takimiya, *Adv. Mater.* **2008**, 20, 3388.
- [51] Y. Tsutsui, G. Schweicher, B. Chattopadhyay, T. Sakurai, J.-B. Arlin, C. Ruzié, A. Aliev, A. Ciesielski, S. Colella, A. R. Kennedy, V. Lemaire, Y. Olivier, R. Hadji, L. Sanguinet, F. Castet, S. Osella, D. Dudenko, D. Beljonne, J. Cornil, P. Samorì, S. Seki, Y. H. Geerts, *Adv. Mater.* **2016**, 28, 7106.
- [52] C. N. Warwick, D. Venkateshvaran, H. Sirringhaus, *APL Mater.* **2015**, 3, 096104.
- [53] G. Giri, E. Verploegen, S. C. B. Mannsfeld, S. Atahan-Evrenk, D. H. Kim, S. Y. Lee, H. A. Becerril, A. Aspuru-Guzik, M. F. Toney, Z. Bao, *Nature* **2011**, 480, 504.
- [54] T. Kubo, R. Häusermann, J. Tsurumi, J. Soeda, Y. Okada, Y. Yamashita, N. Akamatsu, A. Shishido, C. Mitsui, T. Okamoto, S. Yanagisawa, H. Matsui, J. Takeya, *Nat. Commun.* **2016**, 7, 11156.
- [55] K. Sakai, Y. Okada, S. Kitaoka, J. Tsurumi, Y. Ohishi, A. Fujiwara, K. Takimiya, J. Takeya, *Phys. Rev. Lett.* **2013**, 110, 096603.
- [56] J. Wang, R. M. Wolf, J. W. Caldwell, P. A. Kollman, D. A. Case, *J. Comput. Chem.* **2004**, 25, 1157.
- [57] F. Müller-Plathe, *J. Chem. Phys.* **1997**, 106, 6082.
- [58] X.-Y. Mi, X. Yu, K.-L. Yao, X. Huang, N. Yang, J.-T. Lü, *Nano Lett.* **2015**, 15, 5229.
- [59] K. Biswas, J. He, I. D. Blum, C.-I. Wu, T. P. Hogan, D. N. Seidman, V. P. Dravid, M. G. Kanatzidis, *Nature* **2012**, 489, 414.
- [60] C. Chang, M. Wu, D. He, Y. Pei, C.-F. Wu, X. Wu, H. Yu, F. Zhu, K. Wang, Y. Chen, L. Huang, J.-F. Li, J. He, L.-D. Zhao, *Science* **2018**, 360, 778.
- [61] W. Shi, G. Wu, K. Hippalgaonkar, J.-S. Wang, J. Xu, S.-W. Yang, *J. Am. Chem. Soc.* **2018**, 140, 13200.
- [62] E.-G. Kim, J.-L. Brédas, *J. Am. Chem. Soc.* **2008**, 130, 16880.
- [63] J.-M. Zhuo, L.-H. Zhao, P.-J. Chia, W.-S. Sim, R. H. Friend, P. K. H. Ho, *Phys. Rev. Lett.* **2008**, 100, 186601.
- [64] B. Cho, K. S. Park, J. Baek, H. S. Oh, Y.-E. K. Lee, M. M. Sung, *Nano Lett.* **2014**, 14, 3321.
- [65] G. Henkelman, A. Arnaldsson, H. Jónsson, *Comput. Mater. Sci.* **2006**, 36, 354.
- [66] R. Franz, G. Wiedemann, *Ann. Phys. Chem.* **1853**, 165, 497.
- [67] J. Liu, X. Wang, D. Li, N. E. Coates, R. A. Segalman, D. G. Cahill, *Macromolecules* **2015**, 48, 585.
- [68] A. Weathers, Z. U. Khan, R. Brooke, D. Evans, M. T. Pettes, J. W. Andreasen, X. Crispin, L. Shi, *Adv. Mater.* **2015**, 27, 2101.
- [69] T. Park, C. Park, B. Kim, H. Shin, E. Kim, *Energy Environ. Sci.* **2013**, 6, 788.
- [70] Y.-J. Lin, C.-L. Tsai, Y.-C. Su, D.-S. Liu, *Appl. Phys. Lett.* **2012**, 100, 253302.
- [71] H. Okuzaki, M. Ishihara, S. Ashizawa, *Synth. Met.* **2003**, 137, 947.
- [72] S. Ashizawa, Y. Shinohara, H. Shindo, Y. Watanabe, H. Okuzaki, *Synth. Met.* **2005**, 153, 41.
- [73] H. Brooks, *Theory of the Electrical Properties of Germanium and Silicon*, Academic, San Diego, CA **1955**.
- [74] O. D. Restrepo, K. Varga, S. T. Pantelides, *Appl. Phys. Lett.* **2009**, 94, 212103.
- [75] S. Lee, D. C. Paine, K. K. Gleason, *Adv. Funct. Mater.* **2014**, 24, 7187.
- [76] C. Tanase, E. J. Meijer, P. W. M. Blom, D. M. De Leeuw, *Phys. Rev. Lett.* **2003**, 91, 216601.
- [77] C. Luo, A. K. K. Kyaw, L. A. Perez, S. Patel, M. Wang, B. Grimm, G. C. Bazan, E. J. Kramer, A. J. Heeger, *Nano Lett.* **2014**, 14, 2764.
- [78] X. Xu, J. Chen, J. Zhou, B. Li, *Adv. Mater.* **2018**, 30, 1705544.
- [79] W. Shi, Z. Shuai, D. Wang, *Adv. Funct. Mater.* **2017**, 27, 1702847.
- [80] D. B. Mergenthaler, M. Pietralla, S. Roy, H. G. Kilian, *Macromolecules* **1992**, 25, 3500.
- [81] J. C. Duda, P. E. Hopkins, Y. Shen, M. C. Gupta, *Appl. Phys. Lett.* **2013**, 102, 251912.
- [82] C. L. Choy, Y. W. Wong, G. W. Yang, T. Kanamoto, *J. Polym. Sci., Part B: Polym. Phys.* **1999**, 37, 3359.

- [83] S. Shen, A. Henry, J. Tong, R. Zheng, G. Chen, *Nat. Nanotechnol.* **2010**, *5*, 251.
- [84] X. Wang, V. Ho, R. A. Segalman, D. G. Cahill, *Macromolecules* **2013**, *46*, 4937.
- [85] V. Singh, T. L. Bougher, A. Weathers, Y. Cai, K. Bi, M. T. Pettes, S. A. Mcmenamin, W. Lv, D. P. Resler, T. R. Gattuso, D. H. Altman, K. H. Sandhage, L. Shi, A. Henry, B. A. Cola, *Nat. Nanotechnol.* **2014**, *9*, 384.
- [86] R. Shrestha, P. Li, B. Chatterjee, T. Zheng, X. Wu, Z. Liu, T. Luo, S. Choi, K. Hippalgaonkar, M. P. De Boer, S. Shen, *Nat. Commun.* **2018**, *9*, 1664.
- [87] P. Li, L. Hu, A. J. H. Mcgaughey, S. Shen, *Adv. Mater.* **2014**, *26*, 1065.
- [88] A. Shanker, C. Li, G.-H. Kim, D. Gidley, K. P. Pipe, J. Kim, *Sci. Adv.* **2017**, *3*, e1700342.
- [89] L. Wang, Z. Zhang, Y. Liu, B. Wang, L. Fang, J. Qiu, K. Zhang, S. Wang, *Nat. Commun.* **2018**, *9*, 3817.
- [90] S. Baroni, S. De Gironcoli, A. Dal Corso, P. Giannozzi, *Rev. Mod. Phys.* **2001**, *73*, 515.
- [91] J. Noffsinger, F. Giustino, B. D. Malone, C.-H. Park, S. G. Louie, M. L. Cohen, *Comput. Phys. Commun.* **2010**, *181*, 2140.
- [92] J. Xi, D. Wang, Y. Yi, Z. Shuai, *J. Chem. Phys.* **2014**, *141*, 034704.
- [93] J. Xi, D. Wang, Z. Shuai, *Wiley Interdiscip. Rev.: Comput. Mol. Sci.* **2015**, *5*, 215.
- [94] Y. Nakamura, T. Zhao, J. Xi, W. Shi, D. Wang, Z. Shuai, *Adv. Electron. Mater.* **2017**, *3*, 1700143.
- [95] T. Zhao, Y. Sun, Z. Shuai, D. Wang, *Chem. Mater.* **2017**, *29*, 6261.
- [96] a) N. Vukmirović, C. Bruder, V. M. Stojanović, *Phys. Rev. Lett.* **2012**, *109*, 126407; b) N.-E. Lee, J.-J. Zhou, L. A. Agapito, M. Bernardi, *Phys. Rev. B* **2018**, *97*, 115203.
- [97] M. Casula, M. Calandra, G. Profeta, F. Mauri, *Phys. Rev. Lett.* **2011**, *107*, 137006.
- [98] G. Samsonidze, B. Kozinsky, *Adv. Energy Mater.* **2018**, *8*, 1800246.
- [99] Z. Shuai, L. Wang, Q. Li, *Adv. Mater.* **2011**, *23*, 1145.
- [100] S. D. Kang, G. J. Snyder, *Nat. Mater.* **2017**, *16*, 252.
- [101] D. Mendels, N. Tessler, *J. Phys. Chem. Lett.* **2014**, *5*, 3247.
- [102] S. Ihnatsenka, X. Crispin, I. V. Zozoulenko, *Phys. Rev. B* **2015**, *92*, 035201.
- [103] N. Lu, L. Li, M. Liu, *Phys. Chem. Chem. Phys.* **2016**, *18*, 19503.
- [104] B. T. Mcgrail, A. Sehirlioglu, E. Pentzer, *Angew. Chem., Int. Ed.* **2015**, *54*, 1710.
- [105] Y. Du, S. Z. Shen, K. Cai, P. S. Casey, *Prog. Polym. Sci.* **2012**, *37*, 820.
- [106] H. Wang, J.-H. Hsu, S.-I. Yi, S. L. Kim, K. Choi, G. Yang, C. Yu, *Adv. Mater.* **2015**, *27*, 6855.
- [107] C. Cho, K. L. Wallace, P. Tzeng, J.-H. Hsu, C. Yu, J. C. Grunlan, *Adv. Energy Mater.* **2016**, *6*, 1502168.
- [108] T. Zhao, D. Wang, Z. Shuai, *Synth. Met.* **2017**, *225*, 108.